Adsorption and desorption studies of ^{4}He on Nuclepore by capacitance techniques

K. M. Godshalk and R. B. Hallock
Laboratory for Low Temperature Physics, Department of Physics and Astronomy, University of Massachusetts, Amherst, Massachusetts 01003
(Received 16 July 1987)

Measurements of the adsorption and desorption of ^{4}He on the porous polycarbonate substrate Nuclepore are reported for nominal pore diameters of 30, 50, 80, and 200 nm. The isotherms are measured directly by a newly developed capacitance technique. The theory of Saam and Cole, relevant to capillary condensation in cylindrical pores, is examined and confirmed by the data. Pore distributions for the several Nuclepore samples are determined by two techniques.

I. INTRODUCTION

There has been much interest lately in the properties of ^{4}He adsorbed in disordered or porous materials.[1-9] We report here studies of helium films adsorbed on the porous polycarbonate substrate Nuclepore.[10] This work is motivated by a desire to further our understanding of capillary condensation in cylindrical pores and to better characterize the Nuclepore substrate.

We have measured the adsorption isotherms of ^{4}He adsorbed on Nuclepore with nominal pore diameters 30, 50, 80, and 200 nm. The amount of helium adsorbed in the pores is measured directly by a capacitive technique.[5] An analysis of the adsorption isotherms in the low-pressure region ($0 \lesssim P/P_0 \lesssim 0.4$) using the Langmuir and Brunauer-Emmett-Teller (BET) (Ref. 11) theories yields the change in capacitance corresponding to monolayer and second-layer coverages, respectively. A simple model of the capacitance is used to deduce the pore radius from the change in capacitance at monolayer and second-layer completion.

Hysteretic capillary condensation is seen in the high-pressure region ($0.4 \lesssim P/P_0 \lesssim 1$), corresponding to helium film thicknesses (on glass) of $3.2 \lesssim h \lesssim 14$ atomic layers. Saam and Cole[12] (SC) have developed a theory based on the thermodynamic and hydrodynamic properties of the adsorbed film, which predicts the observed hysteresis. We have investigated this hysteresis for 80- and 200-nm-pore-diam Nuclepore in an earlier work.[5] In the present work we have made extensive measurements in the *interior* of the hysteresis loop, in addition to measurements around the hysteresis loop itself. The data taken in the interior of the hysteresis loop provide information which can be used to calculate a pore-size distribution for each Nuclepore sample. These distributions are compared to the distributions derived from fits to the outer, overall, hysteresis loop. We find that the two distributions agree very well; capillary condensation in Nuclepore is consistent with the theory of Saam and Cole.[12]

In the next section we describe the Nuclepore substrate and details of the experiment. The low-pressure region and the corresponding analysis of the data are presented in Sec. III. Section IV describes the region of capillary condensation and contains an analysis in terms of the SC theory.

II. EXPERIMENT

The Nuclepore[10] substrates used here are polycarbonate filters manufactured by an irradiation and etching process. The pores produced are narrow, roughly cylindrical, and oriented[13] at angles $\theta \lesssim 34°$ from the normal to the plane of the filter (Fig. 1). The manufacturer's specifications for the filters used are shown in Table I.

Our experiments were carried out at a temperature of 1.64 K in a conventional regulated pumped-bath Dewar. The sample chamber is a cylindrical brass can which contains the four Nuclepore samples, a glass slide, and a film reservoir of 7 cm^3 of nominal 0.05-μm-diam packed alumina powder to stabilize the film thickness. The capacitors are made by evaporating 500 Å of Ag onto the Nuclepore; the capacitor plates have an area of 1.53 cm^2, with the geometry shown in Fig. 2. Scanning-electron-microscope (SEM) pictures show that the Ag does not block the pores or measurably change the pore diameter. The pore density ξ_M measured from the scanning-electron-microscope pictures differs from the nominal manufacturer's value ξ; the measured values are also given in Table I. The details of the apparatus, the preparation of the samples, and the measurement techniques have been described elsewhere[5] and we will not repeat them in detail here. For pressures below 6.3 torr the pressure is measured using a differential pressure gauge. We measured either the absolute pressure, by pumping with a diffusion pump on the reference side of the pressure gauge, or the pressure difference between the sample cell and a small separate cell maintained at the saturated vapor pressure and mounted 2 cm above the sample cell. For pressures greater than 6.3 torr a superfluid film is present so that third sound will propagate. In this region we measure the third-sound velocity on glass by means of pulsed techniques and derive the pressure from the known properties of third sound on glass. The third-sound velocity C_3 is given by[5,14]

$$C_3^2 = \frac{\rho_s}{\rho}\left[1-\frac{D}{h}\right]\left[1+\frac{TS}{L}\right]^2 \frac{\alpha\beta(3\beta+4h)}{h^3(h+\beta)^2}\ , \qquad (1a)$$

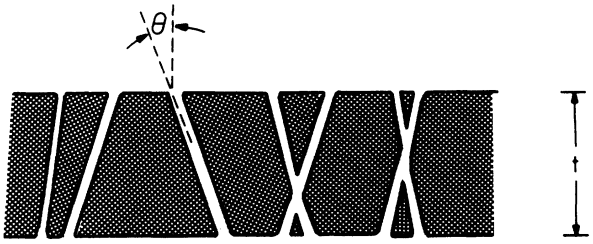

FIG. 1. A schematic diagram of the cross section of a Nuclepore filter (not to scale). The filter thickness is given by t, and the pores are oriented at angles $\theta \lesssim 34°$.

and h is related to P/P_0 by

$$\frac{h^4}{\beta}+h^3=\frac{\alpha}{T\ln(P_0/P)} . \tag{1b}$$

Thus, measurements of C_3 imply values for P/P_0. Here ρ_s/ρ is the bulk superfluid density, D is a parameter which describes the "solid layer," T is the temperature, S is the entropy, and L is the latent heat. The film thickness is given by h, α is the van der Waals constant, and β is a parameter related to retardation effects[15] present for thick films. The parameter D is given empirically for glass[16] as $D=0.5+1.13T(\rho/\rho_s)$; α and β have been measured for glass,[14] with $\alpha=27$ (layer)^3 K and $\beta=41.7$ atomic layers.

III. LOW-PRESSURE REGION

To begin this experiment, the sample chamber was evacuated by diffusion pump at room temperature for 16 h. The samples were then cooled to 1.64 K and the capacitance for each sample was measured. This capacitance with no helium in the cell was termed C_e; C_e is 588.303, 569.571, 587.511, and 316.126 pF (all ± 0.01) for the 30-, 50-, 80-, and 200-nm pore diameters, respectively. The capacitance of the 200-nm sample is different in magnitude from the other three samples due to the different filter thickness (Table I). Gas was then added to the sample cell through a 0.5-m length of room-temperature capillary with a pressure difference of roughly 75 torr across the capillary. The capillary had an experimentally determined effective inner radius of 0.043 cm. Equilibrium times varied from 5 d at extremely low pressure (~ 0.001 torr) to a day or less for slightly higher pressures ($P \gtrsim 0.007$ torr).

The capacitance as a function of pressure is shown in

TABLE I. Characteristics of the Nuclepore filters used in this work. t is the nominal filter thickness in μm, ξ is the nominal pore density expressed in units of 10^8 per cm^2, and ξ_M is the pore density determined from SEM images of the surfaces of the filters.

	Nominal pore diameter (nm)			
	30	50	80	200
t (μm)	6	6	6	10
ξ (10^8 cm^{-2})	6	6	6	3
ξ_M (10^8 cm^{-2})	9.4	7.9	9.0	3.8

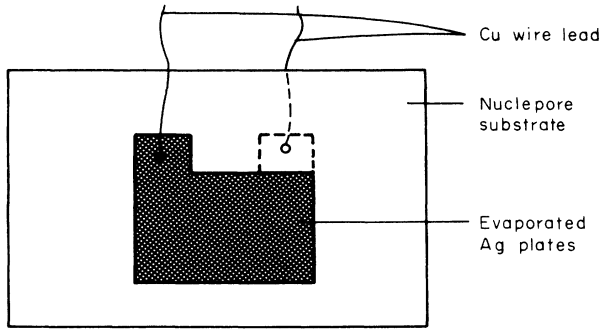

FIG. 2. Schematic representation of the capacitor evaporated directly onto the Nuclepore.

Fig. 3. The capacitance is reported as $\hat{C}=(C-C_e)/(C_f-C_e)$, where C is the capacitance, C_e is the empty capacitance given above, and C_f is the capacitance when the pores are completely filled with liquid helium. The solid line through each isotherm is a fit to the data using the theory described below. Measurements of C_f are described later in the paper; C_f is 588.572 ± 0.004, 570.662 ± 0.007, 588.997 ± 0.01, and 318.118 ± 0.008 pF for the 30-, 50-, 80-, and 200-nm nominal pore diameters, respectively.

In monolayer adsorption the surface forces are very short range so that only molecules striking the bare surface are adsorbed. This type of adsorption often obeys the Langmuir equation,[11]

$$x/V=1/(V_M b)+x/V_M , \tag{2}$$

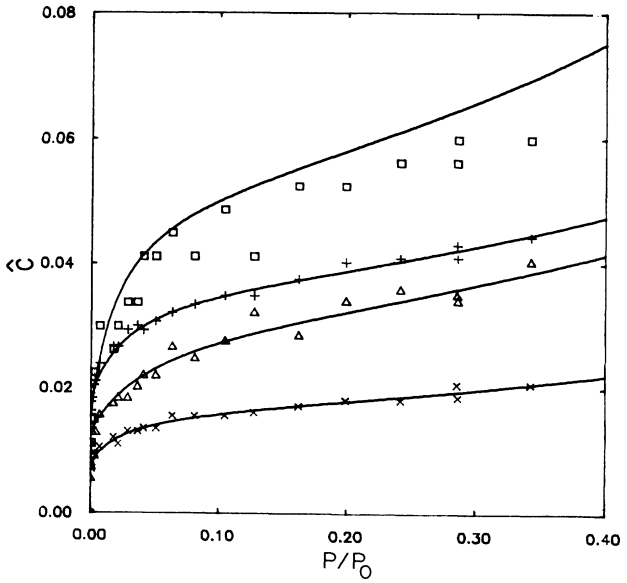

FIG. 3. Capacitance as a function of pressure for the low-pressure region, where $\hat{C}=(C-C_e)/(C_f-C_e)$. The squares denote the 30-nm filter, the triangles the 50 nm, the crosses the 80 nm, and the $\times$'s the 200 nm. The solid lines are a fit to the data using Eq. (5) and the parameters B, δC_1, and δC_2 discussed in the text.

where $x = P/P_0$, P is the pressure, P_0 is the saturated vapor pressure, V is the volume of gas adsorbed at pressure P, V_M is the volume necessary to cover the surface with a complete monolayer, and b is a parameter related to the heat of adsorption. An isotherm is said to obey the Langmuir equation if b is a constant.

In multilayer adsorption, molecules of vapor may be adsorbed on top of already adsorbed molecules; each separate adsorbed layer is assumed to obey a Langmuir equation. Multilayer adsorption obeys the BET equation[11]

$$x/[V(1-x)] = 1/(V_M B) + (B-1)x/(V_M B) , \quad (3)$$

where V_M is again the volume adsorbed at monolayer completion, and B is a parameter related to the energy and entropy of adsorption. For the pressure range $0.05 \lesssim x \lesssim 0.35$, B is approximately a constant for adsorption isotherms which obey the BET equation.

In analyzing helium adsorption data, it is important to realize that the helium-substrate interaction is much stronger than the helium-helium interaction. This causes the monolayer completion to occur at a much lower pressure than for other, more typical situations. Because of this, a BET analysis of the pressure region $0.05 \lesssim x \lesssim 0.35$ actually gives a result corresponding to two adsorbed layers of helium.[17] It is necessary to adjust the theory to account for this fact.

To analyze the capacitance data, we have assumed that the measured capacitance is proportional to the mass of helium adsorbed. The adsorption of the first layer is assumed to follow the Langmuir isotherm. The second layer is assumed to be adsorbed according to the BET equation, except that V must be replaced by $V - V_M$ to give the amount adsorbed after the first layer. V_M in the BET equation [Eq. (3)] now becomes V_2, the volume necessary to complete the second layer. Rewriting Eqs. (2) and (3) in terms of capacitance and with the above modifications gives

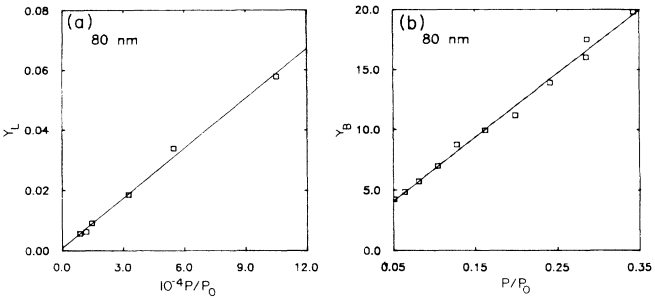

FIG. 4. Langmuir and BET fits to the 80-nm data for finding the capacitance at monolayer and second-layer completion. (a) Langmuir plot: $Y = (P/P_0)/\hat{C}$ as a function of P/P_0. (b) BET plot: $Y = P/P_0/[(\hat{C} - \delta C_1)(1 - P/P_0)]$ as a function of P/P_0. The parameters b, δC_1, B, and C_2 are found from the slope and intercept of these plots.

$$Y_L = \frac{X}{\hat{C}} = \frac{X}{\delta C_1} + \frac{1}{b'\delta C_1} , \quad (4)$$

$$Y_B = \frac{X}{(\hat{C} - \delta C_1)(1-X)} = \frac{1}{B'\delta C_2} + \frac{(B'-1)X}{B'\delta C_2} , \quad (5)$$

where δC_1 and δC_2 are the fractional changes in capacitance associated with the monolayer or second layer, respectively. Here b' and B' are related to the b and B of Eqs. (2) and (3).

The results of this analysis are shown in Fig. 4 for 80 nm; the other pore sizes give similar results. In all cases the data near zero pressure are noisy; as a result the parameter δC_1 has a 20% error. This error causes a 20% error in δC_2 and B'. The fits to the data resulting from

TABLE II. Parameters associated with the analysis of the adsorption measurements. δC_i represents the percent change in capacitance associated with the creation of the ith complete monolayer during adsorption. The parameters b' and B' are defined in Eqs. (4) and (5). $A'(\delta C_1)$ is a measurement of the surface area (cm^2) inside the pores per cm^2 of the flat Nuclepore surface as deduced from measurements of monolayer completion, δC_1. $A'(m)$ is the geometric area per cm^2 calculated from the manufacturer's nominal specifications. $A'(G)$ is the area inside the pore per cm^2 of flat surface deduced from the nitrogen adsorption isotherm technique reported in Ref. 17. To determine $A'(G)$ the results in Ref. 17 have been corrected using the values of ξ and pore radius R in Ref. 17, so that the flat surface area is not included. $R(\delta C_1)$ is the pore radius deduced from the δC_i measurements under the assumption that the pore are perfect nonintersecting cylinders as described in the text. $R(\Delta C)$ is the pore radius deduced from the total change in capacitance from empty to full pores, as described in Sec. IV A.

	Nominal pore diameter (nm)			
	30	50	80	200
δC_1	0.0149	0.0130	0.0181	0.0080
b'	15 479	74 553	60 098	58 130
δC_2	0.0316	0.0184	0.0184	0.0088
B'	59.11	20.60	37.27	37.36
$A'(\delta C_1)$	3.93	12.68	23.96	39.43
$A'(m)$	3.39	5.65	9.05	18.85
$A'(G)$	13.72	13.78	22.94	29.68
$R(\delta C_1)$ (nm)	11.0	42.5	70.0	156.6
$R(\delta C_2)$ (nm)	30.12	77.66	91.88	221.3
$R(\Delta C)$ (nm)	27.0	59.5	64.8	143.3

this analysis are shown in Fig. 3 as solid lines. Table II gives the parameters for each of the fits. To deduce the surface area from the values of δC_1 and δC_2 a simple model for the capacitance is used. The model assumes the pores are perfect, nonintersecting cylinders, that the electric potential is uniform across the capacitor plate, and that the adsorbed helium looks like dielectric added in parallel with the Nuclepore. This gives

$$C - C_e = (\epsilon - 1) A_F / t \ , \tag{6}$$

where ϵ is the dielectric constant of liquid ^{4}He, A_F is the total exposed area of the adsorbed ^{4}He film viewed perpendicular to the plane of the Nuclepore (Fig. 5), and t is the thickness of the Nuclepore. The total surface area A_s inside the pores can be found by using $A_F t \cong A_s d$, where d is the thickness of the adsorbed helium layer in the pore. The value of ϵ must be calculated for each layer based on the density of liquid helium for that layer. The areal density of the first layer is 0.110 Å^{-2}, and the areal density of the second layer is 0.0865 Å^{-2}. The Clausius-Mossotti equation then gives dielectric constants of 1.099 and 1.068 for the first and second layer, respectively.

The results for the surface area using the above model and δC_1 are given in Table II as $A'(\delta C_1)$, where $A'(\delta C_1)$ is the surface area inside the pore per unit area of flat surface. These surface areas are larger than the geometric surface area $A'(m)$ calculated using the manufacturer's specifications. This is not unexpected, since earlier nitrogen adsorption isotherms on Nuclepore[17,18] found similar results $A'(G)$; for comparison these results are given in Table II. The surface areas found by the two different methods agree rather well, except for the 30-nm Nuclepore. For the 30-nm case, it was difficult to determine the parameters for the Langmuir fit, with the result that $2.74 < A'(\delta C_1) < 4.11$. The capacitance model outlined above assumes that the surfaces of the Nuclepore are smooth; any surface roughness[19] would increase the calculated surface area. The pores may also be slightly barrel shaped,[20] so that the interior of the pore is larger than the pore opening. Since the manufacturer specifies the size of the pore openings, the actual surface area is probably larger than that calculated using the nominal value of the pore size.

To determine the pore radii, we assume the pores are smooth, perfect cylinders. This gives $A_s = A_{\rm cap} \xi 2\pi R t$, where $A_{\rm cap}$ is the area of the capacitor plate, ξ is the density of pores, R is the pore radius, and t is the filter thickness. The radii determined here are generally larger than the manufacturer's nominal radius, due to the factors discussed above in relation to the surface area. The pore radii calculated with this model are also given in Table II. We have given the radii calculated using δC_1 and δC_2, corresponding to the monolayer and second-layer completion. These radii also have a 20% error due to difficulty in determining δC_1.

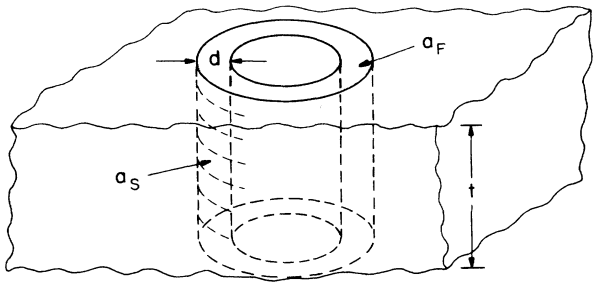

FIG. 5. Schematic diagram relevant to the definition of A_F and A_S discussed in the text, where $A_F = a_F \xi A_{\rm cap}$ and $A_s = a_s \xi A_{\rm cap}$.

IV. DISCUSSION

A. Capillary condensation and hysteresis

In the region of reduced pressure $0.4 \lesssim P/P_0 \lesssim 1.0$, corresponding to film thicknesses h on glass of $3.2 \lesssim h \lesssim 14$, we encounter capillary condensation. The pressure in this region is derived from the measured third-sound velocity on glass and Eq. (1). For the adsorption isotherms, gas is added in discrete amounts through a capillary by applying a pressure difference of 250 torr across the capillary described in the preceding section. For the desorption measurements, gas was pumped out with a roughing pump through a cold trap by metering a valve. The measured isotherms for each of the pore sizes are shown in Fig. 6. The isotherms are given as $\hat{C} = (C - C_e)/(C_f - C_e)$ versus the reduced pressure P/P_0, where the values of C_e and C_f have been given in Sec. III. The total change in capacitance encountered when completely filling the pores, $\Delta C = C_f - C_e$, can be used with Eq. (6) to find a value of

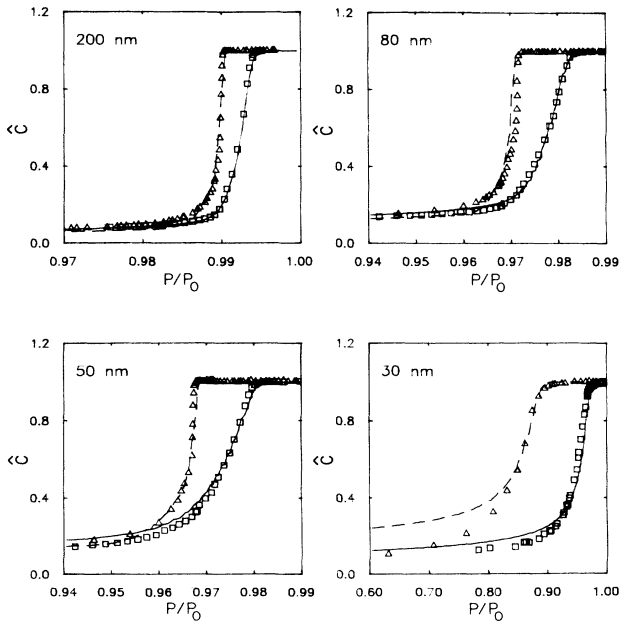

FIG. 6. $\hat{C}$ as a function of pressure in the hysteretic region, where the squares denote adsorption and the triangles denote desorption. The dashed and solid lines are fits to the data using the SC theory, as outlined in the text.

the average pore radius. In this case $A_F=\pi R^2\xi A_{\rm cap}$ and the pore radius R may be found if one knows ΔC, ϵ, t, ξ, and $A_{\rm cap}$. Here $A_{\rm cap}$ is 1.53 cm^2. The results of such a calculation are given in Table II with the designation $R(\Delta C)$.

The hysteretic capillary condensation of ^{4}He adsorbed in cylindrical pores has been examined by Saam and Cole.[12] Nuclepore has roughly cylindrical pores and relatively uniform pore sizes, and is therefore a reasonably good substrate for testing the theory. To model the adsorbed film, SC assume van der Waals forces between the substrate and the film. They calculate the van der Waals potential $U(A)$ for a cylindrical geometry by assuming the potential is the sum of pair interactions of the form $-c/r^6$. Saam and Cole use this model to calculate the thermodynamic and hydrodynamic properties of ^{4}He film adsorbed in a cylindrical pore. They find the film thickness at which it is energetically favorable for the pore to capillary condense, and also find a region in which the film configuration is metastable. The observed hysteresis is due to the presence of this metastability.

At low pressures, or low film coverages, the film lines the pore as shown in configuration I of Fig. 7. As the pressure is increased to the metastable pressure P_M, the film radius A decreases to the radius A_M, at which point configuration I becomes metastable relative to configuration II of Fig. 7. In the metastable region, configuration II has a lower free energy than configuration I but cannot be reached except by a macroscopic deformation of configuration I. As the pressure is further increased, the film radius eventually reaches the critical radius A_c for capillary condensation and the pore will fill with liquid ^{4}He. Any increase in pressure beyond the critical pressure P_c will only increase the film thickness on the flat surface. If the pressure is then decreased from this point, the pore will remain condensed as the pressure decreases below the critical pressure P_c. When the pressure is decreased to the metastable pressure P_M, the pore will begin to empty. At P_M the pores will empty at constant pressure until the film returns to configuration I.

The metastable and critical film radii are given by

$$\left.\frac{dU(A)}{dA}\right|_{A=A_c}=\frac{v_l\sigma}{A_c^2}\ , \tag{7}$$

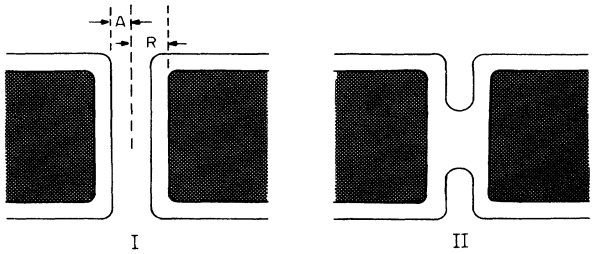

FIG. 7. Film configurations in the pore. Configuration I shows the film during adsorption, in which a film lines the pore. A is the radius of the film surface as measured from the center of the pore, and R is the pore radius. Configuration II shows the probable film configuration during desorption, in which a portion of the pore is condensed, as predicted by SC.

$$\frac{3\pi\alpha}{R_0^2}=-A_MU(A_M)+\frac{2}{A_M}\int_0^{A_M}AU(A)dA\ , \tag{8}$$

where $U(A)$ is the van der Waals potential, $R_0=(3\pi\alpha/\sigma v_l)^{1/2}$, α is the van der Waals constant for Nuclepore, σ is the surface tension of ^{4}He, and v_l is the volume of a liquid ^{4}He atom. The filling fraction, or fraction of the pore volume filled with ^{4}He, for a collection of pores of radius R is

$$X=(R^2-A^2)/R^2=1-Y^2\ , \tag{9}$$

where $Y=A/R$. The reduced pressure here is

$$p=\frac{P}{P_0}=\exp\left[-\frac{R_TR_0^2}{R}\left[-\frac{RU(A)}{3\pi\alpha}+\frac{1}{R_0^2Y}\right]\right]\ , \tag{10}$$

where $R_T=\beta\sigma v_l$. The predicted adsorption isotherm for a single pore radius, $X(p,R)$, can be found numerically from Eqs. (9) and (10). The adsorption isotherm $X_+(p)$ for a distribution in pore sizes is found by summing the contributions of the condensed and uncondensed pores at the pressure p. The result is

$$X_+(p)=\frac{\int_0^{R_c(p)}dR\ R^2S(R)+\int_{R_c(p)}^{\infty}dR\ R^2S(R)X(p,R)}{\int_0^{\infty}dR\ R^2S(R)} \tag{11}$$

where $S(R)$ is the pore size distribution function and $R_c(p)$ is the solution of $P_c[R_c(p)]=p$. $R_c(p)$ is a monotonically increasing function of p, which gives the pore radius $R_c(p)$ which is just becoming critical for a film in equilibrium at pressure p. At pressure p, pores with radii smaller than $R_c(p)$ will be condensed. Similar arguments apply to desorption in the presence of a distribution in pore sizes, and the desorption isotherm $X_-(p)$ is given by

$$X_-(p)=\frac{\int_0^{R_M(p)}dR\ R^2S(R)+\int_{R_M(p)}^{\infty}dR\ R^2S(R)X(p,R)}{\int_0^{\infty}dR\ R^2S(R)} \tag{12}$$

where $R_M(p)$ is defined by $P_M[R_M(p)]=p$.

Equations (11) and (12) predict the adsorption and desorption isotherms in the presence of a pore-size distribution $S(R)$. Third-sound data taken on Nuclepore, however, shows that the pores condense at lower pressures than expected theoretically. This early condensation is apparently due to vibrations in the experimental apparatus and fluctuations caused by the addition of finite doses of ^{4}He gas. Therefore, at a reduced pressure p, pores with radii $R\le R_c(p)+\delta$ have condensed, where δ is a parameter indicating the difference between the theoretical and experimental condensation. Equation (11) for the adsorption then becomes

$$X_+(p)=\frac{\int_0^{R_c(p)+\delta} dR\, R^2 S(R)+\int_{R_c(p)+\delta}^{\infty} dR\, R^2 S(R) X(p,R)}{\int_0^{\infty} dR\, R^2 S(R)} . \tag{13}$$

δ has been measured[4] with third-sound data for the 200-nm Nuclepore. The third-sound data gives δ as a difference in film thickness on glass; this value is then converted into a pore radius difference. We found δ to be 6.0, 9.6, 12.2, and 23.6 nm for the 30-, 50-, 80-, and 200-nm nominal pore diameters, respectively. We used Eqs. (12) and (13) to fit the hysteresis loops on Nuclepore, and thereby deduce pore-size distributions for Nuclepore. The resulting fits are shown in Fig. 6 as solid and dashed lines; the pore-size distributions are shown in Fig. 8 (without data points) as solid and dashed lines, along with other distributions (with data points) to be discussed next.

B. Interior of hysteresis loops

The above discussion refers to continuous adsorption and desorption to completion. Additional information can be gained by filling the pores to some pressure P_d where $X_+(p_d)<1$, and then decreasing the pressure. Studies of such restricted hysteresis curves allow an alternate determination of the pore-size distributions. At P_d a certain fraction of the pores have just reached their critical pressure, and pores with radii $R<R_c(p_d)+\delta$ have condensed. When the pressure is now decreased, the pressure must be reduced to the metastable pressure for these pores before the regular desorption curve is followed for all pores. The filling fraction $X_d(p)$ for desorption from the pressure P_d is

$$X_d(p)=\frac{\int_0^{R_c(p_d)+\delta} dR\, R^2 S(R)+\int_{R_c(p_d)+\delta}^{\infty} dR\, R^2 S(R) X(p,R)}{\int_0^{\infty} dR\, R^2 S(R)} . \tag{14}$$

At the pressure $P_M[R_c(p_d)]$, $X_d(p)$ will meet and follow the regular desorption curve given by $X_-(p)$.

Measurements of this type provide information about the fraction of pores becoming critical at the pressure P_d, and can be used to determine the distribution $S_+(R)$. The subscript $+$ denotes a distribution determined by increasing the pressure to the point P_d and then decreasing the pressure to measure $X_d(p)$. Using Eqs. (13) and (14) one finds

$$\frac{d}{dp}[X_+(p)-X_d(p)]\bigg|_{p=p_d}=R^2 S_+(R)\frac{dR_c(p)}{dp}\left[\frac{1-X(p,R)}{\int_0^{\infty} dR\, R^2 S(R)}\right]\bigg|_{p=p_d,\ R=R_c(p_d)} . \tag{15}$$

A similar situation occurs if one begins with all the pores condensed and decreases the pressure to P_a [corresponding to a point $X_-(P_a)<1$ on the desorption curve] and then increases the pressure. In this situation, pores with radius $R>R_M(p_a)$ have already begun to empty. When the pressure is now increased, those pores that have begun to empty will begin to fill, while the pores with radii $R<R_M(p_a)$ will remain condensed. The filling fraction $X_a(p)$ in this case is

$$X_a(p)=\frac{\int_0^{R_M(p_a)} dR\, R^2 S(R)+\int_{R_M(p_a)}^{\infty} dR\, R^2 S(R) X(p,R)}{\int_0^{\infty} dR\, R^2 S(R)} , \tag{16}$$

and one finds for the distribution $S_-(R)$,

$$\frac{d}{dp}[X_-(p)-X_a(p)]\bigg|_{p=p_a}=R^2 S_-(R)\frac{dR_M(p)}{dp}\left[\frac{1-X(p,R)}{\int_0^{\infty} dR\, R^2 S(R)}\right]\bigg|_{p=p_a,R=R_M(p_a)} . \tag{17}$$

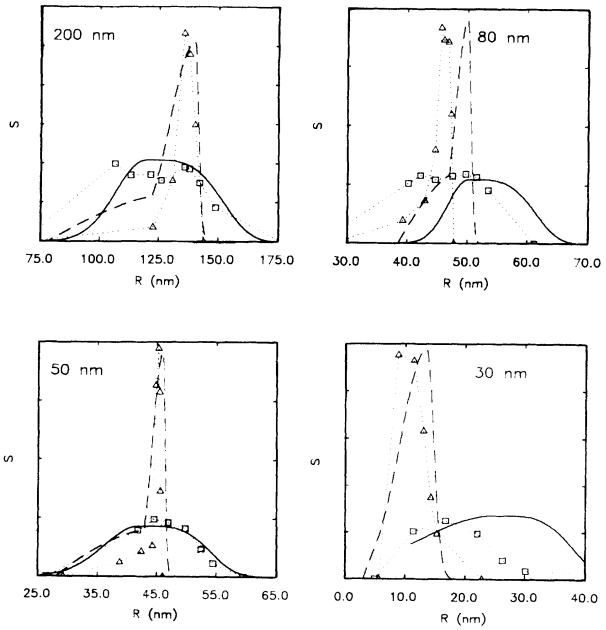

FIG. 8. Distributions in pore size, in arbitrary units. The solid line is the distribution from the adsorption part of the hysteresis loop; the dashed line is the distribution from the desorption part of the hysteresis loop. The squares are the distribution S_+ determined from Eq. (15) and the triangles are the distribution S_- determined from Eq. (17). A dotted line has been drawn through the symbols as a guide to the eye.

If the pores are not perfectly cylindrical, the distributions $S_+(R)$ and $S_-(R)$ deduced from Eqs. (15) and (17) will not be identical. This is because the adsorption and desorption isotherms are governed by different regions of the pore.

We have taken measurements of such restricted hysteresis curves, and thus collected data in the interior of each overall hysteresis loop in order to determine the pore distribution as described above. A set of such measurements is shown in Figs. 9(a) and 9(b) for the 200-nm-nominal-diam pore. Each interior curve (X_d or X_a) yields one point in the pore-size distribution. The value of the distribution for that particular curve is found by measuring the slope of the interior curve X_d (X_a) at the pressure P_d (P_a) and the slope of the regular adsorption (desorption) curve at the pressure P_d (P_a). These measurements are used on the left-hand side of Eq. (15) [Eq. (17)]. The value of the pore-size distribution S_+ (S_-) can then be found, since the other quantities in the equation are given theoretically. In determining the pore-size distribution S_+ for adsorption, the parameter δ discussed in the preceding section must be used. The distribution calculated from Eq. (15) must be shifted by the amount δ to larger radii. The pore-size distributions calculated from Eqs. (15) and (17) are shown in Fig. 8, with the solid symbols which have been connected by dotted lines as a guide to the eye. The distributions calculated using data from the interior of the hysteresis loops agree remarkably well with the distributions derived from the outer hysteresis loops and Eqs. (12) and (13) (shown with solid and dashed lines in Fig. 8). This consistency is a good confirmation of the theory of Saam and Cole.[12]

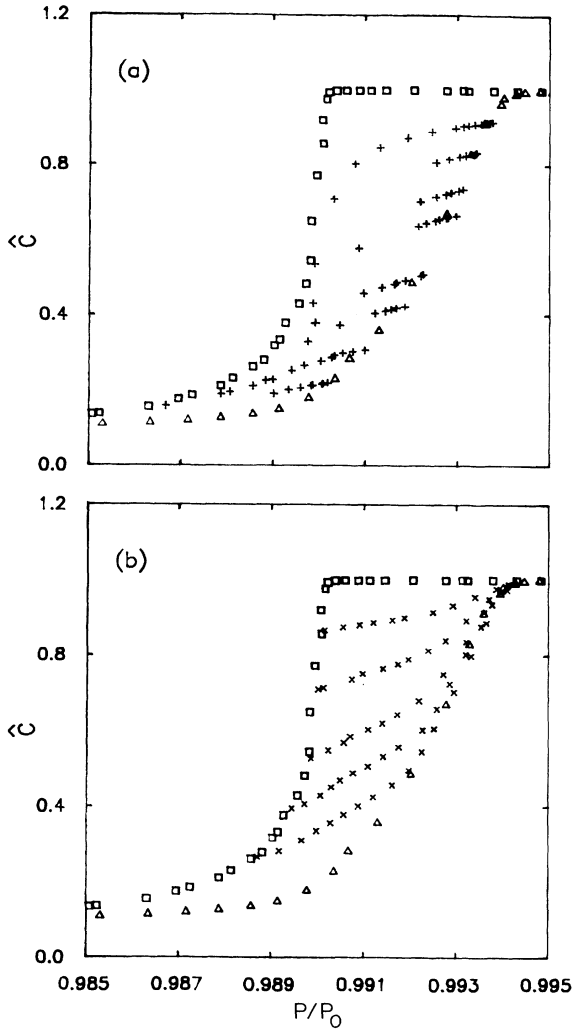

FIG. 9. Data taken in the interior of the hysteresis loop for the 200 nm Nuclepore. The squares and triangles denote the data taken *around* the hysteresis loop during a run separate from that during which data in the interior of the hysteresis loop were collected. In Fig. 9(a), the crosses denote $X_d(p)$—data taken by adding to a pressure p_d on the adsorption curve and then subtracting gas. In Fig. 8(b), the $\times$'s denote $X_a(p)$—data taken by pumping out to a pressure p_a on the desorption curve and then adding gas.

V. CONCLUSIONS

We have used a new capacitive technique[5] to measure the adsorption isotherms of ^{4}He adsorbed on Nuclepore of four different pore sizes. This technique is quite sensitive, and we have used it to perform a Langmuir (Ref. 11) and BET (Ref. 11) analysis of the low-pressure data. This analysis yielded values for the surface area *inside* the pores of the Nuclepore filter. Capillary condensation and hysteresis are seen in the high-pressure region of each isotherm. This hysteresis is predicted by Saam and

Cole,[12] and the theory agrees very well with experiment. Saam and Cole theory also provides two separate methods for determining a distribution in pore sizes, and the distributions determined from each method are consistent with each other. We have thus seen that the capacitive technique is very useful for measuring adsorption isotherms, and that the theory of Saam and Cole[12] provides a very good explanation of capillary condensation of ^{4}He in Nuclepore.

ACKNOWLEDGMENTS

We have benefited from conversations with D. T. Smith. This work was supported by the National Science Foundation under Grant No. DMR 85-17939.

[1]V. Kotsubo and G. A. Williams, Phys. Rev. B **33**, 6106 (1986); R. Rosenbaum, G. A. Williams, D. Heckerman, J. Marcus, D. Scholler, J. Maynard, and I. Rudnick, J. Low Temp. Phys. **37**, 663 (1979).
[2]B. K. Bhattacharyya and F. M. Gasparini, Phys. Rev. B **31**, 2719 (1985).
[3]R. Rosenbaum, G. A. Williams, D. Heckerman, J. Marcus, D. Scholler, J. Maynard, and I. Rudnick, J. Low Temp. Phys. **37**, 663 (1979).
[4]J. M. Valles, Jr., D. T. Smith, and R. B. Hallock, Phys. Rev. Lett. **54**, 1528 (1985).
[5]D. T. Smith, K. Godshalk, and R. B. Hallock, Phys. Rev. B **36**, 202 (1987).
[6]D. T. Smith and R. B. Hallock, Phys. Rev. B **34**, 226 (1986).
[7]D. T. Smith, C. Lorenson, and R. B. Hallock, Jpn. J. Appl. Phys. **26**, Suppl. 26-3 285 (1987).
[8]D. J. Bishop, J. E. Berthold, J. M. Parpia, and J. D. Reppy, Phys. Rev. B **24**, 5047 (1981).
[9]B. C. Crooker, B. Hebral, E. N. Smith. Y. Tokano, and J. D. Reppy, Phys. Rev. Lett. **51**, 666 (1983).
[10]Nuclepore Corporation, Pleasanton, CA.
[11]E. A. Flood, *The Solid Gas Interface* (Dekker, New York, 1967).
[12]W. F. Saam and M. W. Cole, Phys. Rev. B **11**, 1086 (1975).
[13]D. Peterson (private communication).
[14]S. Putterman, *Superfluid Hydrodynamics* (North-Holland, Amsterdam, 1974), Chap. V.
[15]E. S. Sabisky and C. H. Anderson, Phys. Rev. A **7**, 790 (1973).
[16]J. H. Sholtz, E. O. McLean, and I. Rudnick, Phys. Rev. Lett. **32**, 147 (1974). In this reference T should be removed from the expression for D.
[17]T. P. Chen, M. J. DiPirro, A. A. Gaeta, and F. M. Gasparini, J. Low. Temp. Phys. **26**, 927 (1977).
[18]T. P. Chen *et al.*, Rev. Sci. Instrum. **51**, 846 (1980).
[19]F. M. Gasparini (unpublished).
[20]D. S. Cannel (private communication).